Astron. Astrophys. 320, 196–208 (1997)

ASTRONOMY AND ASTROPHYSICS

Radiation driven wind models for A, F and G supergiants

L. Achmad[1,2⋆], **H.J.G.L.M. Lamers**[2,3], **and L. Pasquini**[1]

[1] European Southern Observatory, Casilla 19001, Santiago, Chile
[2] SRON Laboratory for Space Research, Sorbonnelaan 2, 3584 CA Utrecht, The Netherlands
[3] Astronomical Institute, Princetonplein 5, 3584 CC Utrecht, The Netherlands

Received 2 April 1996 / Accepted 1 August 1996

Abstract. We investigate the effects of radiation pressure on the atmospheres of A, F and G-supergiants by calculating hydrodynamical model atmospheres for stars with $5500 \leq T_{\rm eff} \leq 9500$ K. In the subsonic part of the wind, the radiation pressure by continuum and lines from Kurucz (1992) is taken into account. In the supersonic part of the wind, the radiation pressure is expressed in terms of the force multiplier formalism (Castor et al. 1975) with the correction for the finite disk taken into account. The temperature structure is from the $T(\tau)$ relation of blanketed model atmospheres.

The predicted mass loss rates of the A-supergiants agrees excellently with the observed values. However the predicted terminal velocities are about a factor 3 higher than observed. We discuss several possible causes for this discrepancy. The most likely one is a change in the force multiplier parameter α of the line radiation force from about 0.5 in the lower parts of the wind to a much smaller value of about 0.1 throughout most of the wind. This might be the result of a change in the ionization of the wind with distance, or a decoupling of the line driven ions in the wind from the ambient gas.

The predicted mass loss rate of the G-type supergiant 22 Vul, which is the only G-supergiant with a reliable mass loss rate, is a factor 10^5 smaller than observed. This is probably due to the fact that G-supergiants have chromospheres, which were not taken into account in our model. Our models for F-supergiants could not be compared with observations because there are no reliable empirical mass loss rates or terminal wind velocities for normal F-supergiants. The F-supergiants ρ Cas and HR 8752 have highly variable mass loss rates which obviously cannot be explained by our models.

We conclude that mass loss from A-type supergiants is most likely due to a line driven wind but that the mass loss from G-supergiants is not. It is interesting to find the spectral type between F0 and G3 where the radiation driven wind models break down and to compare that with the type where the chromospheres become noticeable.

The high opacity in the hydrogen ionization zone produces a net outward force in those layers. This gives rise to a pressure inversion in the subsonic part of the atmosphere, but does not lead to high mass loss rates.

Key words: stars: atmospheres – stars: mass-loss – supergiants – hydrodynamics

1. Introduction

Hydrostatic model atmospheres of supergiants may show pressure inversions in the layers where the outward directed radiation force is larger than the inward directed force of the gravity. This is easily seen in the equation of hydrostatic equilibrium:

$$\frac{dP_{\rm gas}}{dr} = -\rho g + \frac{\pi\rho}{c}\int_0^\infty \kappa_\nu F_\nu d\nu \qquad (1)$$

This pressure inversion is a result of the equation of hydrostatic equilibrium: if the net force (i.e. the force due to gravity and radiation pressure) is directed outward and the atmosphere is forced to be hydrostatic, this force must be compensated by the force due to an *outward increase in the gas pressure*. A pressure inversion is hence a consequence of the assumption of hydrostatic equilibrium. For G and F-supergiants, the pressure inversion is due to the high opacity in the hydrogen ionization zone deep in the atmosphere (Kurucz, 1992). If the layers above the pressure inversion have enough weight, the layers with the pressure inversion may be stable. However, if the layers above the pressure inversion cannot constrain the motion of the gas, the outward directed net force may give rise to outflow. This might result in a high mass loss rate driven by the continuum opacity of the hydrogen ionization zone. We investigate this possibility.

The CAK model, after its recent improvements, is very good in describing the observed winds and mass loss of hot stars. However, in the subsonic region, the CAK formalism predicts much too low radiative pressure and thus badly reproduces the subsonic atmospheric structure. This is especially true for the F & G-supergiants where the hydrostatic Kurucz's models (1992)

Send offprint requests to: L. Achmad

⋆ On leave from Department of Astronomy, ITB, Ganesha 10, Bandung 40132, Indonesia.

show high pressure inversion in the photosphere. Our motivation is to investigate the mass loss rates and velocity structures of the A, F & G-supergiants that include both the subsonic and supersonic radiation pressures. In the subsonic region the radiative acceleration is calculated using Kurucz model atmospheres (Kurucz, 1992), and it is connected to the CAK formalism (Castor et al. 1975, Abbott 1982) in the supersonic region. With these accelerations, we construct the radiation driven wind model atmospheres for A, F & G-supergiants. We also investigate the existence of the pressure inversion in the hydrodynamic model.

We discuss the pressure inversion in hydrostatic models of $T_{\rm eff}$ between 5500 K and 9500 K in Sect. 2. The calculation of the simple hydrodynamical model atmospheres is described in Sect. 3. In Sect. 4 we describe the calculation of radiation driven wind models where the radiation pressure in the subsonic and supersonic regions are both taken into account. In Sects. 5 & 6, we discuss the mass loss rates and the terminal velocities of radiation driven wind models for A, F and G-supergiants and we compare them with observations for a few stars in Sect. 7. The conclusions are in Sect. 8.

This is the second paper in a series about mass loss from F & G-supergiants. In the first paper (Lamers & Achmad, 1994) we studied the effect of mass loss on the spectroscopic turbulence derived from line profile studies. We showed that the "turbulence" could in fact due to the presence of a velocity gradient in the atmosphere due to mass loss, if the mass loss rate is high.

Table 1. Kurucz's model atmosphere with P-inversion

	location of the P-inversion ($\tau_{\rm Ross}$)*			
Temp. (K)	log $g_{\rm grav}$: 0.0	0.5	1.0	1.5
5250	7.8	x	x	x
5500	3.3	x	x	x
5750	3.3	4.4	x	x
6000	2.5	3.3	56.1	x
6250	—	2.5	3.3	x
6500	—	1.8	2.5	17.9
6750	—	1.4	2.5	5.7
7000	—	1.0	1.8	2.5
7250	—	0.8	1.4	2.4
7500	—	0.6	1.0	1.8
7750	—	—	0.8	1.8
8000	—	—	0.57	x
8250	—	—	0.56	x

$-$: indicates that no hydrostatic models exist for this combination of $T_{\rm eff}$ and $g_{\rm grav}$.
x : indicates that no P-inversion occurred at the model with this combination of $T_{\rm eff}$ and $g_{\rm grav}$.
Remark :
* the location of the P-inversion is indicated by the Rosseland optical depth where $P_{\rm gas}$ reaches its highest value at the top of the inversion layer.

2. The pressure inversion in hydrostatic model atmospheres

We first investigate the occurrence of pressure inversions in hydrostatic atmospheres of F & G-supergiants. We adopt the LTE plane-parallel model atmospheres from Kurucz (1992) that include the opacity of millions of lines.

In Table 1 we tabulate all Kurucz's model atmospheres which have a P-inversion. The table shows that pressure inversions occur in hydrostatic models between $5250 \leq T_{\rm eff} \leq 8250$ K at low gravities of $0.0 \leq \log g_{\rm grav} \leq 1.5$, but not at higher gravities. In this temperature range, the ionization of hydrogen, which produces a strong peak in the opacity, occurs in the photosphere. Due to this *high opacity*, the value of the right hand side of Eq. (1) becomes positive, which results in the outward increase of the gas pressure (P-inversion). Table 1 also shows the location of the pressure inversion. The quantity listed is the Rosseland optical depth where $P_{\rm gas}$ reaches its highest value at the top of the P-inversion layer. We see that the optical depth of the top of the P-inversion layer increases towards lower effective temperature. This is a consequence of the increasing depth of the ionization zone with decreasing $T_{\rm eff}$. For models with an effective temperature higher than 8250 K, the ionizing layers of hydrogen do not generate a P-inversion although some models still show a ρ-inversion. The existence of the ρ-inversion has been reviewed by Maeder (1992).

In Fig. 1 we show the run of $P_{\rm gas}(\tau_{\rm Ross})$ of Kurucz's hydrostatic model with $T_{\rm eff}$ = 7500 K and log $g_{\rm grav}$ = 0.5 in which the P-inversion occurs. It can be seen clearly that the peak of the opacity occurs in the ionization zone of hydrogen, which in this model is at $\tau_{\rm Ross} \sim 1$. The peak of $\kappa_{\rm Ross}$ also coincides with the steepest outward increase of $P_{\rm gas}$, as expected on the basis of Eq. (1). This figure shows clearly that the radiative acceleration in the subsonic region of these stars are very high, higher than the gravity.

3. Hydrodynamical model atmospheres

For the purpose of this study we calculate simple extended hydrodynamical model atmospheres. In this section we describe the assumptions.

3.1. The adopted temperature structure

For our simplified models we want to use a $T(\tau)$ relation that fits accurately to those calculated for extended line-blanketed model atmospheres. For that purpose we compare several $T(\tau)$ relations to that of an extended line blanketed model, kindly provided to us by Plez (1994), for a star of $T_{\rm eff}$ = 5500 K and log $g_{\rm grav}$ = 0. This comparison is shown in Fig. 2, in which we plotted the $T(\tau)$ relations of four models :

a. the line-blanketed extended model of Plez (1994).
b. the line-blanketed plane-parallel model of Kurucz (1992).
c. the grey extended model of Lamers & Achmad (1994), based on the assumption of frequency independent Eddington factors as suggested by Wessolowski et al. (1988).

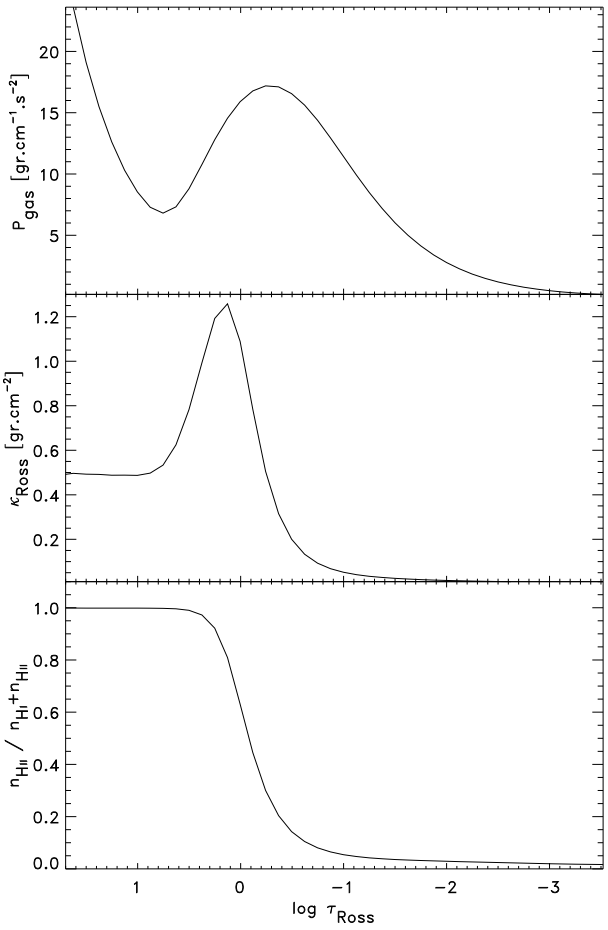

Fig. 1. The upper graph: the P-inversion of hydrostatic model of Kurucz with $T_{\rm eff}$ = 7500 K and $\log g = 0.5$; the middle graph: the Rosseland absorption coefficient ($\kappa_{\rm Ross}$) and the lower graph: the ionization fraction of hydrogen. Notice that the 'bump' in $\kappa_{\rm Ross}$ is related to the hydrogen ionization zone and that the peak of $\kappa_{\rm Ross}$ coincides with the steepest outward increase of $P_{\rm gas}$.

d. a grey plane-parallel model with :

$$T^4(\tau) = {T_{\rm eff}}^4 \left(\frac{3}{4}\tau + \frac{1}{2}\right) \ . \qquad (2)$$

The comparison between models (c) and (d) shows the effect of the spherical extension of a grey atmospheres. Spherical extension has only a minor effect on the $T(\tau)$ relation. The comparison between model (b) and (d) shows the very strong influence of line blanketing on the models. The comparison between the extended blanketed model (a) and the plane-parallel blanketed model (b) shows that the $T(\tau)$ relation of extended blanketed models is very similar to that of the plane-parallel blanketed models of Kurucz (1992).

In the temperature range we are interested in, the only grid of blanketed models that is available is the one from Kurucz (1992) for plane-parallel atmospheres. Since the results above showed that the $T(\tau)$ relation of such a model is very similar to that of an extended blanketed model, we decided to use the temperature structure from the plane-parallel models. So for each hydrodynamical model we used the $T(\tau)$ relation from the plane-parallel line-blanketed model of Kurucz with the same values of $T_{\rm eff}$ and $\log g_{\rm grav}$.

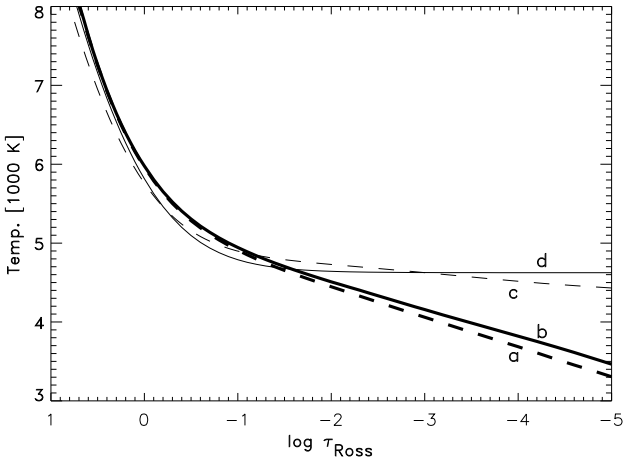

Fig. 2. Temperature structures of different models of the same $T_{\rm eff}$ and $\log g$: (a) thick-dashed line is the line-blanketed extended atmosphere, (b) thick-solid line is the line blanketed plane-parallel atmosphere, (c) thin-dashed line is the grey extended atmosphere, and (d) thin-solid line is the grey plane-parallel atmosphere. Notice that the effect of line-blanketing is more important than the sphericity effect.

We have to note that in the supersonic part of the wind, the $T(\tau)$ relation from static models is not expected to be very accurate since it ignores the adiabatic cooling. However, the temperature of the wind does not play a strong role in determining the structure of the wind.

3.2. The velocity structure

The velocity structure of the atmosphere is given by the Newton's law, which is :

$$\frac{dv}{dt} = -\frac{GM_\star}{r^2} - \frac{1}{\rho}\frac{dP_{\rm gas}}{dr} + g_{\rm ext} \ , \qquad (3)$$

where v is velocity structure, $M_\star$ is mass of the star, G is the gravitational constant, r is the distance from the centre of the star, ρ is the density and $P_{\rm gas}$ is the gas pressure. The $g_{\rm ext}$ describes any external accelerations, e.g. the radiative acceleration due to continuum opacity or/and the radiative acceleration due to lines (g_ℓ).

We assume that the outflow from the star is radial and in a steady state. With the help of the equation of the conservation of mass :

$$\dot{M} = 4\pi r^2 \rho v \ , \qquad (4)$$

where $\dot{M}$ is the mass loss rate, and under the assumption that the flow behaves like a perfect gas :

$$P_{\rm gas} = \frac{R}{\mu}\rho T \ , \qquad (5)$$

where R is the gas constant, μ is the mean atomic weight and T is temperature, we can write the momentum Eq. (3) as :

$$(v^2 - a^2)\frac{1}{v}\frac{dv}{dr} = -\frac{GM_\star}{r^2} + \frac{2a^2}{r} - \frac{R}{\mu}\left(\frac{dT}{dr} - \frac{T}{\mu}\frac{d\mu}{dr}\right) + g_{\rm ext} \ . \quad (6)$$

In this equation, a is a local isothermal sound velocity defined as :

$$a(r) = \sqrt{\frac{RT(r)}{\mu(r)}} \ . \quad (7)$$

The velocity structure is obtained by solving the momentum equation of Eq. (6). This equation can be solved only if $\mu(r)$ is known a-priori. On the other hand $\mu(r)$ itself can only be calculated if the values of $T(r)$ and $\rho(r)$ are known, assuming that the ionization is in LTE.

In order to overcome the above problem, we use an iterative way in solving Eq. (6). For the first iteration, we use $T(r)$ and $\rho(r)$ from the original Kurucz's model to calculate $\mu(r)$. With these $T(r)$ and $\mu(r)$ we solve the momentum Eq. (6) to obtain a velocity structure $v(r)$. Then a *new* density structure, $\rho(r)$, is calculated from this $v(r)$ (see Sect. 3.3). With the new $T(r)$ and $\rho(r)$ we recalculate a new $\mu(r)$ and we solve the momentum Eq. (6) again. The procedure is iterated until $v(r)$ converges.

Another problem in solving Eq. (6) concerns the sonic point of the momentum equation, where $v(r) = a(r)$. We want a solution of $v(r)$ that is subsonic deep in the atmosphere and supersonic at the outer part. In order to obtain a finite positive value of dv/dr at the sonic point, the right hand side of Eq. (6) has to increase outward from a negative value to a positive value at the sonic point, and it has to reach zero exactly at the sonic point. Therefore we start the integration of the momentum equation (Eq. 6) at the sonic point and integrate both inwards and outwards. So the Eq. (6) is solved in two parts: from the sonic point outward and inward.

Following the Eq. (6), the sonic point is the critical point as long as $g_{\rm ext}$ is not a function of dv/dr. Due to the nature of our computation, where Eq. (6) is solved by iteration and $g_{\rm ext}(r)$ is fixed and is calculated using parameters from the previous iteration (see Sect. 4.4), our critical point is always the same as the sonic point even if $g_{\rm ext}$ were a function of dv/dr (e.g. radiative line driven winds). The fact that the solution converges, as we will show later, means that the approach is correct. In the formulation of the CAK theory, their critical point lays further out than the sonic point.

3.3. The density structure

The density structure is given by the calculated $v(r)$ in Eq. (6) and the conservation of mass in Eq. (4). But in order to be able to solve this, we need to know the mass loss rate ($\dot{M}$), which we do not know a-priori. In order to estimate the $\dot{M}$, we use the following procedure.

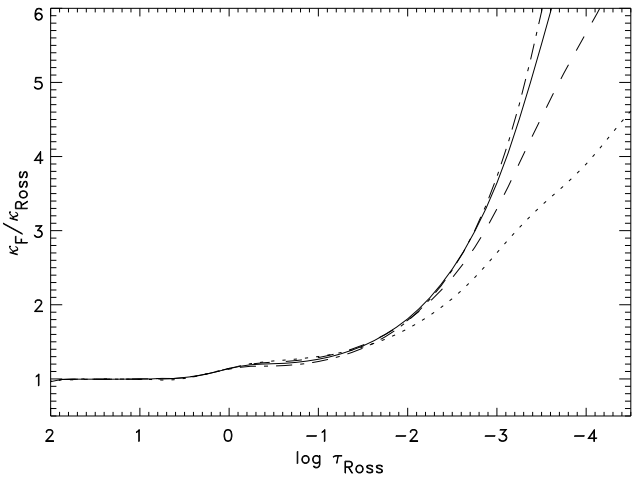

Fig. 3. The ratio of $\overline{\kappa}_{\rm F}/\kappa_{\rm Ross}$ as a function of $\tau_{\rm Ross}$, calculated for $T_{\rm eff}$ = 7500 K of Kurucz's model. Dash-dotted, solid, dashed and dotted lines are for models with log $g_{\rm grav}$ of 2.0, 1.5, 1.0 and 0.5 respectively.

The stellar luminosity $L_\star$ can be approximated by :

$$L_\star = 4\pi {R_\star}^2 \sigma {T_\star}^4, \quad (8)$$

where we adopt that $T_\star$ and $R_\star$ are the temperature and the radius where the Rosseland optical depth $\tau_{\rm Ross}$ is 2/3.

For a given mass loss rate $\dot{M}$ we can calculate $\rho(r)$ and $\tau_{\rm Ross}(r)$. We demand that the Rosseland optical depth is 2/3 in the layer where $T(r) = T_{\rm eff}$. In order to fulfill this demand, we need to adjust the value of $\dot{M}$. This results in values of $\dot{M}$ and $\rho(r)$ simultaneously.

With the new $\rho(r)$, we iterate the calculation of $v(r)$. This iteration is done several times until we obtain consistent values of $v(r)$, $\rho(r)$ and $\dot{M}$ which satisfy the momentum equation, the mass conservation and Eq. (8).

4. Hydrodynamical model with radiative acceleration

4.1. Radiative acceleration in the subsonic region

The radiative acceleration in the subsonic region ($g_{\rm sub}$) can be written as :

$$g_{\rm sub} = -\frac{1}{\rho}\frac{dP_{\rm rad}}{dr} = \frac{\pi}{c}\int_0^\infty \kappa_\nu F_\nu d\nu = \frac{\pi}{c}\overline{\kappa}_{\rm F} F \ , \quad (9)$$

where κ_ν and F_ν are the monochromatic opacity and flux, F is the integrated flux and $\overline{\kappa}_{\rm F}$ is the flux-mean opacity, defined by :

$$\overline{\kappa}_{\rm F} = \frac{1}{F}\int_0^\infty \kappa_\nu F_\nu d\nu \ . \quad (10)$$

The exact calculation of $\overline{\kappa}_{\rm F}(r)$ requires the solution of the radiative transfer equation throughout the atmosphere over the full wavelength range. This is beyond the scope of the models calculated here. Therefore we will adopt an approximation which is sufficiently accurate. We assume that the ratio $\overline{\kappa}_{\rm F}/\kappa_{\rm Ross}$

depends only on the optical depth. The ratio $\overline{\kappa}_{\rm F}/\kappa_{\rm Ross}$ as a function of $\tau_{\rm Ross}$ is calculated from the plane parallel blanketed model atmospheres (Kurucz, 1992) for each value of $T_{\rm eff}$ and $\log g_{\rm grav}$. This value is shown in Fig. 3 for one particular set of models. The ratio approaches 1 at $\tau_{\rm Ross} > 10^{-1}$ as expected, but becomes larger at smaller values of $\tau_{\rm Ross}$.

We adopt these relations between $\overline{\kappa}_{\rm F}/\kappa_{\rm Ross}$ and $\tau_{\rm Ross}$ for our hydrodynamical models. The values of $\kappa_{\rm Ross}(T, P_{\rm gas})$ are taken from Kurucz as well.

4.2. Radiative acceleration in the supersonic region

Castor et al. (1975) have shown that the radiative acceleration by spectral lines in the Sobolev approximation can be described by :

$$g_\ell = CF\frac{\sigma_{\rm e}\,\pi F}{c}\mathscr{M}(t)\ , \tag{11}$$

where $\sigma_{\rm e}$ is the electron scattering opacity, $\pi F = \sigma {T_{\rm eff}}^4$ and CF is the correction factor for the cone finite angle (Pauldrach et al. 1986, Friend & Abbott 1986, see also Kudritzki 1989). The 'force multiplier' $\mathscr{M}(t)$ is approximated by :

$$\mathscr{M}(t) = kt^{-\alpha}\ , \tag{12}$$

where t is an optical depth parameter for an expanding atmosphere, defined by :

$$t = \frac{\sigma_{\rm e}\rho v_{\rm th}}{dv/dr}\ , \tag{13}$$

(Castor et. al. 1975; Abbott 1982). The values of the force multiplier parameters k and α are determined by a power law fit of g_ℓ to t. Abbott (1982) has tabulated the values of k and α as a function of effective temperature from 50 000 K down to 6 000 K, for an assumed normalization constant of $\sigma_{\rm e} = 0.301$. So in the calculation of the line radiative acceleration with Eq. (11) one should use this value for the normalization, even if the real electron scattering coefficient in the atmosphere is smaller.

We do not use the force multiplier parameter δ which represents the change in ionization when going outward in the wind. The value of δ is small, in order of ~ 0.1 (Abbott, 1982). The increase of δ from 0.0 to 0.1 can increase the mass loss rate up to 50% and reduce the terminal velocity around 20% (Kudritzki et al. 1989). Assuming $\delta = 0$ speeds up the iteration considerably and still gives sufficiently accurate wind models for our purpose.

4.3. The combined radiative accelerations

The expression for g_ℓ in Eq. (11) gives the contribution for the radiative acceleration in the hydrodynamic part of the atmosphere, because it is only non-zero in the region of the atmosphere with a velocity gradient. Naturally, it is becoming important somewhere near the sonic point. As for $g_{\rm sub}$ (Eq. 9), it includes the contributions from lines and continuum in the (near)-hydrostatic part of the atmosphere. It is only used in the subsonic region

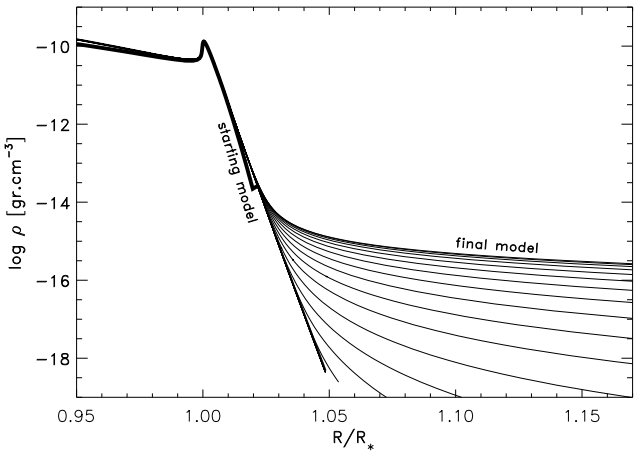

Fig. 4. The density structure of hydrodynamic models during the iteration. The thick-solid line, labeled as 'starting model', is the Kurucz's hydrostatic density structure. The other lines are the hydrodynamic solutions from the first until the last iteration, labeled as 'final model'.

where the Kurucz model atmosphere is still reliable. Except for very high mass loss rates $\gtrsim 10^{-5} M_\odot\ {\rm yr}^{-1}$, we will show later that the value of $g_{\rm sub}$ near the sonic point is already negligible as compared to g_ℓ. For this reason it is safe to assume that that the total radiative acceleration is :

$$g_{\rm ext} = g_{\rm sub} + g_\ell\ , \tag{14}$$

since the $g_{\rm sub}$ and g_ℓ complement one another.

We note that limiting $g_{\rm sub}$ to be valid only in the subsonic region is not reliable for stars with very high mass loss rates, since the location of the sonic point can be very deep in the atmosphere where both $g_{\rm sub}$ and g_ℓ are non-negligible. This will underestimate the mass loss rate. This problem does not occur for our models.

4.4. An example of a model with the radiative acceleration

We calculate the hydrodynamical model of a star with $T_{\rm eff}$ = 7500 K, $R_\star = 232\,R_\odot$ and mass of $M_\star = 19.6\,M_\odot$ ($\log g_{\rm grav}$ = 1.0). This model is chosen because it has a very strong pressure inversion deep in the hydrostatic model atmosphere at $\tau \simeq 1$ (Kurucz, 1992). This means that $g_{\rm grav} - g_{\rm sub} < 0$ at the pressure inversion. We want to know whether the pressure inversion also occurs in a hydrodynamical model.

The radiation pressure is calculated using Eq. (14). As has been mentioned before, because the driving force of the lines depends on ρ and dv/dr, it has to be calculated for each iteration. We start with a hydrostatic model atmosphere from Kurucz and iterate the solution of the equations. We calculate the new velocity structure from the momentum equation (Eq. 6), the new density structure from the continuity equation (Eq. 4) and the requirements that $\tau_{\rm Ross}(R_\star) = 2/3$. These new parameters give a new driving force of the lines. This process is iterated until it converges, which is typically in about 30 to 50 iterations. The final model satisfies the momentum equation, it goes through

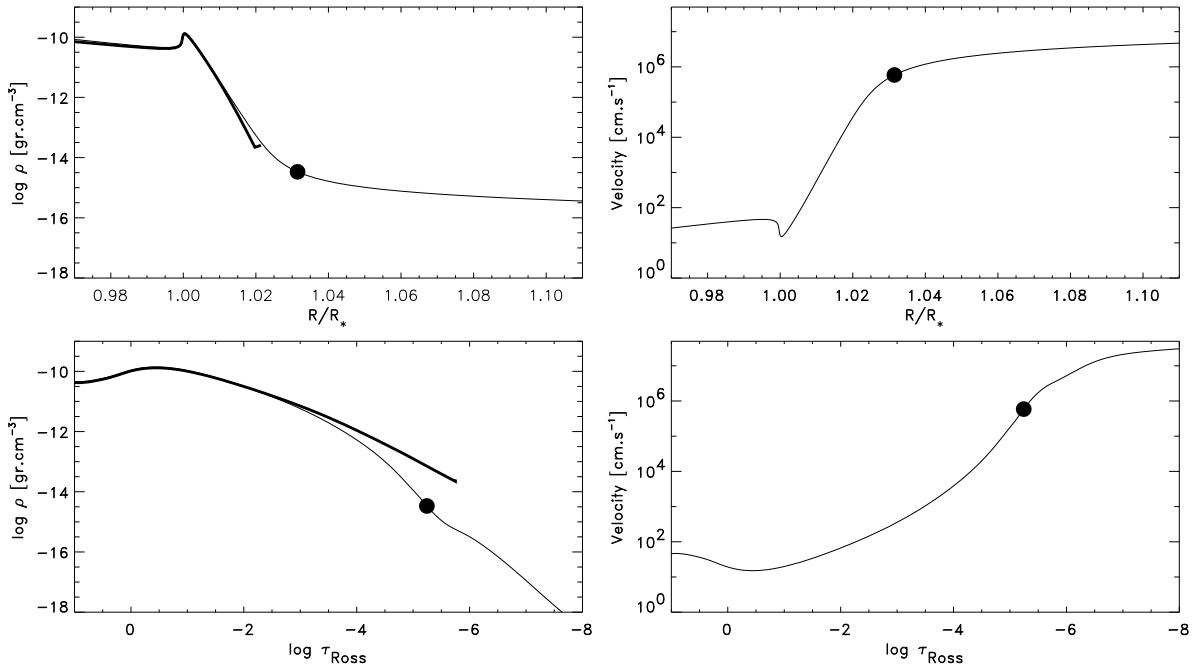

Fig. 5. The $\rho(r)$ and $v(r)$ as functions of radius and optical depth. The thick lines are the hydrostatic plane-parallel model and the thin lines are the hydrodynamic model. The filled circles are the location of the sonic point. Note that the stellar radius corresponds to $\tau_{\rm Ross}$=2/3.

the sonic point, it has the pre-described $T(\tau)$-structure (from the blanketed hydrostatic model) and it reaches $\tau_{\rm Ross} = 2/3$ at the stellar radius where $T(\tau_{\rm Ross} = 2/3) = T_{\rm eff}$. The mass loss rate is the result from the model.

In Fig. 4 we show the progression of the iteration, described above (see also Sect. 3), from the first adopted hydrostatic model to the final model. The final calculated mass loss rate for this star is about $10^{-7}\ M_\odot\ {\rm yr}^{-1}$. Fig. 5 shows the density and velocity structures for the hydrostatic and for the final hydrodynamic model, both as a function of r and as a function of $\tau_{\rm Ross}$. The hydrostatic model stops at $\tau_{\rm Ross} = 10^{-6}$ which is at 1.02 R_*.

Both hydrostatic and hydrodynamic models show the density inversion at $\log \tau_{\rm Ross} \simeq 0$. Since we use the same $T(\tau)$ relation, this shows that the pressure inversion, which exist in the hydrostatic model, also appears in the hydrodynamic model. This shows that *the pressure inversion is real and not an artifact of the hydrostatic assumption*. Notice in Fig. 5 the sonic point is located above the pressure inversion. The situation can be different for star with a much higher mass loss rate where the sonic point is at higher density. If the radial velocity in the hydrogen ionization layers is larger than the local isothermal sound velocity (which means that the sonic point is *below* the ionization layers), the hydrogen ionization will result in a positive value of dv/dr and the pressure inversion will not occur. We estimate that such a star, if exist, would have mass loss rate $\gtrsim 10^{-4.4} M_\odot\ {\rm yr}^{-1}$.

4.5. The effect of the pressure inversion on $\dot{M}$

To estimate the mass loss rate due to the pressure inversion only (or high subsonic radiation pressure), we switch off g_ℓ in Eq. (14) from the model in Sect. 4.4. We now assume that $g_{\rm sub}$ represents the radiation pressure for both subsonic and supersonic region. The result from our calculation shows that the mass loss rate is very low, $\dot{M} \ll 10^{-20} M_\odot\ {\rm yr}^{-1}$. We conclude that the mass loss rate from this star is mainly due to the enhanced radiation pressure by lines in a medium with a velocity gradient (as described in the formalism of CAK), and the contribution of the high radiation pressure deep in the atmosphere (below the sonic point) is negligible to the overall mass loss rate. This result also shows that the $g_{\rm sub}$ is much lower as compared to g_ℓ at the sonic point.

5. Mass loss rates of line driven winds for A, F and G-supergiants

We have calculated line driven wind models for a grid of models with effective temperatures between 5500 and 9500 K and with gravities of log $g_{\rm grav}$ between 0 and 2.5, with the finite cone angle effect taken into account. For each gravity we derived the stellar mass, the radius and the luminosity from the evolutionary models of Maeder & Meynet (1988) of stars with initial masses in the range of 7-80 $M_\odot$. The luminosities are between 5 10^3 and 1.5 10^6 $L_\odot$. The parameters of the models are listed in Table 2. The first six columns give the stellar parameters. Columns (7) to (12) give information about the radiation driven wind models. Column (7) gives the mass loss rate. The location of the sonic point with respect to the stellar radius where $\tau_{\rm Ross} = 2/3$, is listed in column (8). Columns (9), (10) and (11) give a fit of the calculated velocity law to the β-law (see below in Sect. 6.1). Column (12) gives the predicted edge velocity of the strongest UV res-

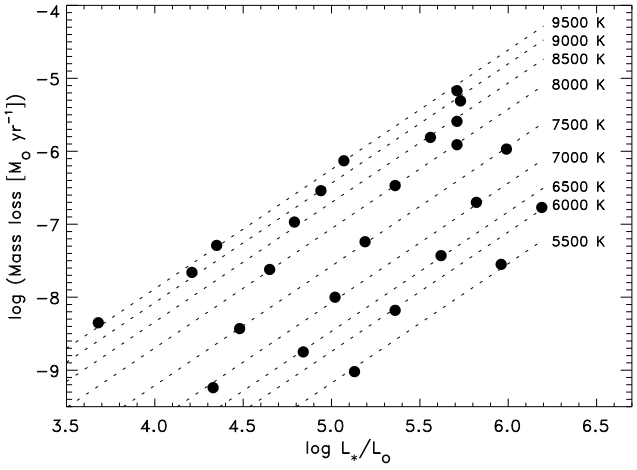

Fig. 6. The mass loss rate of radiation driven wind models for A, F & G-supergiants plotted versus log $L_\star$. Models with different effective temperatures are indicated. Note that the mass loss rates of models with the same value of $T_{\rm eff}$ are on straight lines with a slope independent of $T_{\rm eff}$.

onance lines (see Sect. 6.2). The mass loss rates and terminal velocities predicted by Abbott (1982) are given in columns (13) and (14). The mass loss rates are in $M_\odot$ yr^{-1} and the velocities are in km s^{-1}. In this section we discuss the predicted mass loss rates.

5.1. The predicted mass loss rates

The mass loss rates of our models are plotted versus log $L_\star$ in Fig. 6. The models show the general trend of radiation driven wind models that $\dot{M}$ increases with $L_\star$.

A linear least square fit between $\dot{M}$ and log $L_\star$ for each temperature gives :

$$\log \dot{M} \simeq f(T) + 1.636\ \log(L_\star/L_\odot)\ , \qquad (15)$$

where the values of $f(T)$ is listed in Table 3. The dotted lines in Fig. 6 show the fitting for models with a same temperature. The value of 1.636 in Eq. (15) is the average of the fitting values for the different temperatures. This equation shows that for stars with a same effective temperature, $\dot{M}$ is proportional ${L_\star}^{1.636}$.

5.2. Comparison with Abbott's predictions

Abbott (1982) showed that the $\dot{M}$ is a sensitive function of $L_\star$ as well as of k and α. In fact the constants $f(T)$ in Table 3 is a simple linear function of $\frac{1}{\alpha}\log k$. Abbott has derived an approximate formula for the mass loss rates of line driven winds. Several assumptions were used in this derivation, such as an isothermal atmosphere and the point source model. His mass loss rate formula is :

$$\dot{M} = \frac{\alpha}{V_{\rm th}}\ k^{1/\alpha}\left[\frac{(1-\alpha)\Gamma_\circ}{1-\Gamma}\right]^{(1-\alpha)/\alpha}\left(\frac{L_\star}{c}\right)\ , \qquad (16)$$

Table 3. The values $f(T)$

$T_{\rm eff}$ [K]	$f(T)$
5500	-17.359
6000	-16.925
6500	-16.648
7000	-16.255
7500	-15.755
8000	-15.241
8500	-14.883
9000	-14.620
9500	-14.430

where

$$\Gamma = 7.66\,10^{-5}\ \sigma_{\rm e}\ \frac{L_\star/L_\odot}{M_\star/M_\odot}\ . \qquad (17)$$

$\Gamma_\circ$ is similar to Γ, except $\Gamma_\circ$ uses a constant value of $\sigma_{\rm e} = 0.301$ which comes from the definition of g_ℓ in Eq.(11), while Γ uses a real electron scattering $\sigma_{\rm e}$ which depends on the number of electrons. Since $\Gamma_\circ \sim L_\star/M_\star$ this equation predicts that $\dot{M} \sim {L_\star}^{1/\alpha}\cdot {M_\star}^{(\alpha-1)/\alpha}$. With $\alpha \simeq 0.5$, we expect that the mass loss rate is proportional to ${L_\star}^2\cdot {M_\star}^{-1}$. From our stellar parameters in Table 2, we found that roughly the $L_\star \sim {M_\star}^3$, so the relation of $\dot{M} \sim {L_\star}^{1.636}$ that we found in Eq. (15) is reasonable.

We want to compare our predicted mass loss rates with those predicted by the CAK theory (Eq. 16). The predicted values from the CAK theory are given in the last two columns of Table 2. The mass loss rates of our hydrodynamical models, which use the same values for the force multiplier are typically smaller by 0.20 dex. This is due to two effects: (a) our models include the finite cone angle effect for the radiation pressure whereas Abbott used the point source approximation, and (b) Abbott's models are isothermal whereas our models have the $T(\tau)$-relation of blanketed atmospheres.

In order to investigate the influence of the finite cone angle, we also calculated our models *without* the finite cone angle effect (*CF* correction). We conclude that :

a. The mass loss rates of models with *CF* correction are smaller by about 0.25 dex compared to models without the *CF* correction. This was also found and explained by Pauldrach et al. (1986) and by Friend & Abbott (1986). It is due to the fact that the line radiation pressure in the region below the CAK critical point is smaller than for the point source approximation.

b. Although our models have an extra subsonic force, the mass loss rates, calculated by taking into account the temperature stratification but *without* the *CF* correction, are systematically smaller by about 0.05 dex compared to those calculated using Eq. (16). However in Sect. 4.5 we have shown that the extra subsonic force does not play a strong role in determining the predicted $\dot{M}$ of our models in Table 2. We have checked that the discrepancy is due to the difference in the adopted $T(\tau)$-relation.

Table 2. The calculated mass loss and terminal velocity

						our result						Abbott (1982)	
$T_{\rm eff}$ [K]	$\log g_{\rm grav}$	$M_\star/M_\odot$	$R_\star/R_\odot$	$\log L_\star/L_\odot$	$v_{\rm esc}$	$\log \dot{M}$	$r_{\rm s}/R_\star$	$r_\circ/R_\star{}^{(1)}$	$\beta^{(1)}$	$v_\infty{}^{(1)}$	$v_\infty^{\rm obs(2)}$	$\dot{M}$	v_∞
5500	0.0	40.8	1054	5.96	121	-7.55	1.0783	1.0724	0.78	204	204	-7.41	108
5500	0.5	18.8	404	5.13	133	-9.02	1.0729	1.0696	0.77	227	200	-8.87	118
6000	0.0	47.8	1144	6.19	126	-6.77	1.0676	1.0649	0.78	230	230	-6.61	118
6000	0.5	22.7	444	5.36	140	-8.18	1.0627	1.0574	0.78	261	218	-8.01	130
6500	0.5	29.5	507	5.62	149	-7.43	1.0510	1.0484	0.78	307	307	-7.23	146
6500	1.0	16.1	209	4.84	171	-8.75	1.0437	1.0437	0.77	369	362	-8.53	168
7000	0.5	34.7	549	5.82	155	-6.70	1.0424	1.0398	0.80	356	356	-6.50	159
7000	1.0	17.7	220	5.02	175	-8.00	1.0384	1.0358	0.79	415	415	-7.77	179
7000	1.5	11.0	99	4.33	206	-9.24	1.0315	1.0289	0.79	515	454	-8.93	211
7500	0.5	39.3	584	5.99	160	-5.97	1.0353	1.0327	0.80	390	390	-5.77	170
7500	1.0	19.6	232	5.19	179	-7.24	1.0327	1.0301	0.81	468	468	-7.01	190
7500	1.5	12.3	103	4.48	213	-8.43	1.0269	1.0269	0.79	559	559	-8.16	226
8000[3]	0.8	32.3	373	5.71	182	-5.91	1.0387	1.0387	0.80	469	469	-5.77	198
8000	1.0	22.8	250	5.36	186	-6.47	1.0335	1.0335	0.80	474	474	-6.28	203
8000	1.5	13.9	110	4.65	220	-7.62	1.0232	1.0226	0.82	621	621	-7.42	239
8500[3]	0.9	32.3	330	5.71	193	-5.59	1.0396	1.0396	0.80	481	481	-5.40	212
8500	1.0	28.0	277	5.56	196	-5.81	1.0383	1.0383	0.80	494	494	-5.63	216
8500	1.5	15.4	115	4.79	226	-6.97	1.0266	1.0240	0.80	598	598	-6.81	249
9000[3]	1.0	32.7	300	5.73	204	-5.31	1.0369	1.0369	0.79	501	501	-5.11	224
9000	1.5	16.8	121	4.94	230	-6.54	1.0306	1.0306	0.81	659	659	-6.31	253
9000	2.0	10.1	52.6	4.21	271	-7.66	1.0209	1.0235	0.82	838	838	-7.45	297
9500[3]	1.1	32.3	264	5.71	216	-5.17	1.0340	1.0340	0.79	526	526	-4.95	235
9500[3]	1.5	18.1	127	5.07	233	-6.13	1.0314	1.0314	0.79	595	595	-5.91	254
9500	2.0	11.0	54.9	4.35	276	-7.29	1.0235	1.0235	0.80	759	759	-7.07	301
9500	2.5	6.8	25.5	3.68	319	-8.35	1.0173	1.0148	0.83	947	947	-8.12	348

The mass loss rates are in $M_\odot$ yr^{-1} and the velocities are in km s^{-1}.

Remark :
(1) Values of $R_\star$, β and v_∞ are calculated by fitting a beta-law velocity to our calculated $v(r)$ (see Sect. 6.1).
(2) The predicted edge velocities of the Mg II resonance lines. (see Sect. 6.2).
(3) These models have lower gravities than the lowest gravities available in Kurucz's model.

5.3. An accurate formula for $\dot{M}$

Abbott's (1982) prediction of mass loss rates for the radiative driven winds theory, Eq. (16), suggests that $\dot{M}$ depends on $L_\star$, $M_{\rm eff}$ and on a combination of factors that depend on the force multiplier parameters. Based on these predictions we expect that our $\dot{M}$ is a simple function of $f'(k, \alpha, L_\star, M_{\rm eff})$, where :

$$\begin{aligned} f' &= \frac{1}{\alpha}\log k + \frac{(1-\alpha)}{\alpha}\log\left(\frac{\Gamma_\circ}{1-\Gamma}\right) + \log\left(\frac{L_\star}{L_\odot}\right) \\ &= \frac{1}{\alpha}\log k + \frac{1}{\alpha}\log\left(\frac{L_\star}{L_\odot}\right) + \\ &\quad \frac{(\alpha-1)}{\alpha}\left[4.64 + \log\left(\frac{M_{\rm eff}}{M_\odot}\right)\right] , \end{aligned} \tag{18}$$

with $M_{\rm eff} = M_\star \cdot (1-\Gamma)$.

In Fig. 7 we have plotted our mass loss rate versus $f'(k, \alpha, L_\star, M_{\rm eff})$. The figure shows a very tight relation between $\dot{M}$ and $f'(k, \alpha, L_\star, M_{\rm eff})$. The relation can be fitted with the linear least square fit :

$$\log \dot{M} = -9.55 + f'(k, \alpha, L_\star, M_{\rm eff}) , \tag{19}$$

where $\dot{M}$ is in unit of $M_\odot$ yr^{-1}. This equation fits the mass loss rates of all our models within 0.05 dex.

6. The terminal velocities of the line driven winds

6.1. The predicted terminal velocities

The velocity law of radiation driven wind models is usually described in terms of β-type velocity law :

$$v(r) = v_\circ + (v_\infty - v_\circ)\left(1 - \frac{r_\circ}{r}\right)^\beta . \tag{20}$$

The original radiation driven wind models by Castor, Abbott and Klein (1975) had a velocity law with β=0.5 and $v_\infty/v_{\rm esc}$

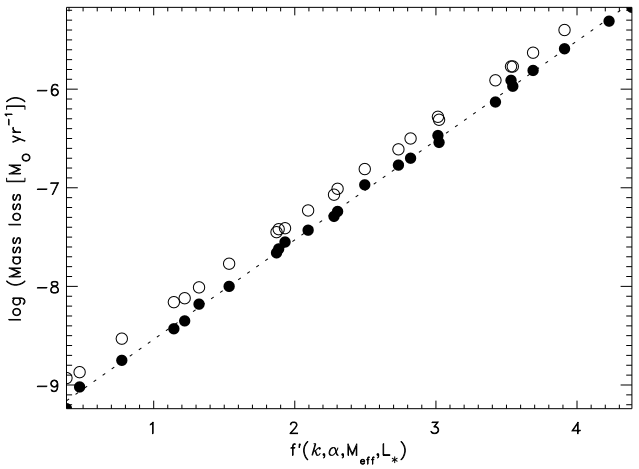

Fig. 7. The mass loss versus $f'(k, \alpha, L_\star, M_{\rm eff})$. Filled circles indicate our non-isothermal models with the *CF* correction. Open circles refer to Abbott's predictions for isothermal winds without the *CF* correction. Our mass loss rates are about 0.3 dex smaller than Abbott's values. This is due to the *CF* effect and the $T(r)$ structure in the wind.

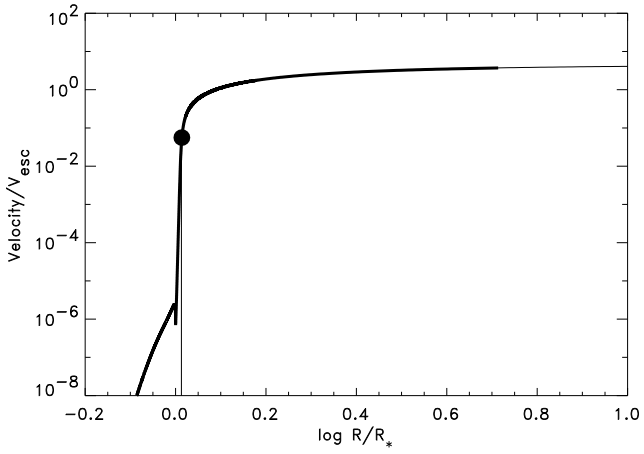

Fig. 8. The fitted beta-law velocity structure (thin line) compared to the calculated velocity structure (thick line). The values of β is 0.81 and the terminal velocity v_∞ is 390 km s^{-1}. Note that the dip at around $R = R_\star$ is due to the pressure inversion. The location of sonic point is marked by a filled circle.

about 3. Later models, in which the *CF* correction was taken into account, showed that $\beta \simeq 0.7$ (Pauldrach et al. 1986).

Our calculations result in a velocity law for each hydrodynamical model. We have fitted the velocity law of each of our models with a slightly simplified β-law of the type :

$$v(r) = v_\infty \left(1 - \frac{r_\circ}{r}\right)^\beta \quad . \tag{21}$$

The fitting is done starting from r slightly higher than $r_{\rm s}$ to $r = 5R_\star$ using the chi-square method, where v_∞, $r_\circ$ and β are the free parameters to be found. In Fig. 8, we show an example of such a fitting for a star with $T_{\rm eff}$ = 7500 K, $R_\star$ = 584 $R_\odot$ and M = 39.3 $M_\odot$ (log $g_{\rm grav}$ = 0.5). The fit matches the calculated velocity law above the sonic point very accurately. The values of $r_\circ/R_\star$, β and v_∞ are given in Table 2, columns (9), (10) and (11). The location of the sonic point $r_{\rm s}/R_\star$ is also given.

Castor et al. (1975) has shown that the terminal velocity of a radiation driven wind in the point source limit scales with the escape velocity as :

$$\frac{{v_\infty}^2}{{v_{\rm esc}}^2} = \frac{\alpha}{1-\alpha} \quad . \tag{22}$$

However, the models with the finite disk correction factor for the radiation pressure included have higher terminal velocities because the mass loss rates are smaller (e.g. Pauldrach et al. 1986). The last column of Table 2 shows the calculated v_∞ with this formula. The terminal velocity of our models is higher than predicted by this formula by about a factor 2.5. In Fig. 9 the value of $v_\infty/v_{\rm esc}$ is plotted as a function of $T_{\rm eff}$.

From our results listed in Table 2, and from Figs. 8 & 9 we conclude that :

a. In most cases the velocity law can be fitted very well with a β-law where β is around 0.8.

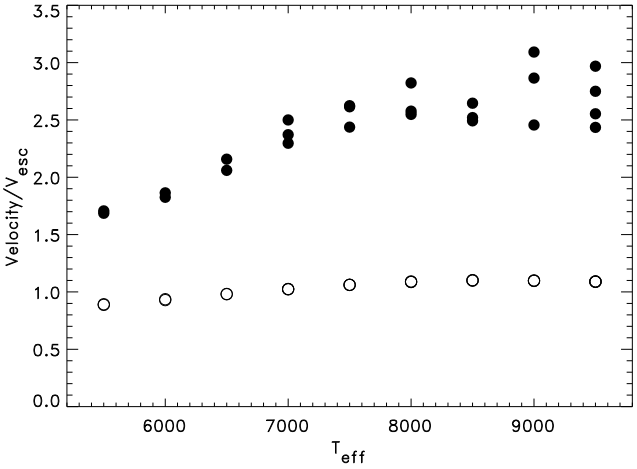

Fig. 9. The predicted ratio $v_\infty/v_{\rm esc}$ as a function of effective temperature for our models. Filled circles indicate our non-isothermal models with the *CF* correction. Open circles refer to Abbott's predictions for isothermal winds without the *CF* correction. The mean predicted ratio decreases from about 2.7 at 9000 K to about 1.7 at 5500 K.

b. The values of v_∞ from our models are about 2 to 2.5 times higher than Abbott's predictions. This is due to the *CF* correction which reduced the mass loss rates. This results in a smaller density *in the wind*. But since the radiative acceleration g_ℓ is proportional to $\rho^{-\alpha}$ (Eqs. 11-13), a smaller ρ gives a larger radiative acceleration in the wind and hence a higher value of v_∞. In other words, the radiative force is acting on a less dense material which gives a higher momentum per gram in the wind and hence gives a higher terminal velocity. Note that the v_∞ of our models *without CF* correction but taking into account the temperature stratification are about 1.4 times higher than Abbott's predictions. This is due to the fact that the outward decrease of $T(r)$ in our models produces a force due to gas

pressure that is not taken into account in deriving Eq. (22) for the isothermal CAK wind models.

6.2. The predicted edge velocity of strong wind lines

In the next section we will compare the results of our hydrodynamical model calculations with observations for a few stars. The observed terminal velocities $v_\infty^{\rm obs}$ are usually derived from violet edge of strong P-Cygni profiles. The lines have to be optically thick far in the wind to represent the true terminal velocity v_∞. The lines most suited for measuring the terminal velocities are the Mg II resonance lines near 2800 Å, because they are optically thick in the winds of cool stars up to large distances.

We have calculated the expected values $v_\infty^{\rm obs}$ of the terminal velocity for our radiation driven wind models, as measured from the Mg II resonance line of 2795.528 Å. The calculation is done by assuming that all Mg ions in the wind are in the form of Mg II and all Mg II ions are in the ground level. The calculated $v_\infty^{\rm obs}$ represents the Doppler velocity where the radial optical depth is unity. Since this velocity is reached at a distance of at least 3 $R_\star$ where the velocity is about constant, the relevant optical depth is :

$$\tau_\nu^\ell = \int_0^r \kappa_\nu^\ell \rho dr = 1. \tag{23}$$

In this equation κ_ν^ℓ is :

$$\kappa_\nu^\ell = \frac{\pi e^2}{mc} f n_{\rm Mg} \phi(\Delta(\nu)) \ , \tag{24}$$

where f is the oscillator strength, $n_{\rm Mg}$ is the number of Mg ions per gram and $\phi(\Delta(\nu))$ is a simple thermal Doppler profile function in co-moving frame where $\Delta(\nu) = \nu\{1 - v(r)/c\} - \nu_\circ$. In these equations, ν is the frequency seen by the observer and $\nu_\circ$ is the frequency at the line centre in the rest-frame.

The resulting values of $v_\infty^{\rm obs}$ are listed in Table 2. It is easy to see from the expression for τ_ν^ℓ that the distance in stellar radii where $\tau_\nu^\ell = 1$ is reached is proportional to $\dot{M}/(R_\star v_\infty)$. The data in Table 2 show that the violet edge of the P-Cygni profile of the Mg II resonance line is a good indicator of v_∞ if $\dot{M}/(R_\star v_\infty)$ is larger than 10^{-13}, with $\dot{M}$ in $M_\odot\,{\rm yr}^{-1}$, v_∞ in ${\rm km\,s}^{-1}$, and $R_\star$ in $R_\odot$. For smaller values of this quantity the violet edge is formed in the layers where the acceleration occurs, so the edge velocity is smaller than the terminal velocity.

7. Comparison with observations

In this section we want to compare our predictions with observed mass loss rates and terminal velocities of A, F and G-supergiants.

Terminal velocities of 117 O,B,A and F-stars have been measured by Lamers et al. (1995) from IUE spectra. Their values with the uncertainty are listed for 13 A-supergiants and one F-supergiant. They are mostly determined from the violet edge of the P-Cygni profiles of the Mg II lines.

The mass loss rates of seven A-type supergiants have been derived from their IR excess and from the UV lines. They are listed in Table 4. Unfortunately there are no reliable mass loss rates for F-supergiants. The compilation of empirical mass loss rates from the literature by de Jager et al. (1988) contains only two F-supergiants hotter than 5500 K. However, one of them (HD 163506 = 89 Her) is in fact a peculiar post AGB binary star and the other one (CRL 2688) is not an F-supergiant but a much cooler AGB star with CO emission in the wind and a wind velocity of only 19.7 ${\rm km\,s}^{-1}$. A third F star, (HD 224014 = ρ Cas) has a highly variable and episodic mass loss rate; de Jager et al. give two mass loss rates which differ by a factor 10^3. The two only G-supergiants with known mass loss rates are HR 8752 and 22 Vul (Reimers, 1989). However, HR 8752 is very similar to ρ Cas in spectroscopic variability and episodic mass loss and cannot be compared to our predictions. This leaves only the star 22 Vul for comparison with our models. The star 22 Vul of spectral type G3 Ib-II is a ζ Aur type binary. The mass loss rate of $6 \times 10^{-9}\ M_\odot\,{\rm yr}^{-1}$ has been derived from the observations of the spectrum of the B-star companion through the wind of 22 Vul as a function of binary phase by Reimers & Che-Bohnenstengel (1986). The terminal velocity of the wind is 160 $\pm$ 20 ${\rm km\,s}^{-1}$. The stellar parameters for this star are from Ake & Parson (1985).

The mass loss rates and the terminal velocities of these A and F-supergiants are listed in Table 4, in order of spectral type. The stellar parameters from Lamers et al. (1995) were adopted for the stars studied by these authors. The stellar parameters of the other stars are from the references quoted in Table 4, and if needed with the help of the evolutionary track of Maeder & Meynet (1988).

7.1. Comparison between observed and predicted mass loss rates

The observed mass loss rates are compared with the predictions in Fig. 10. The agreement between observations and theory is very good. The one G-supergiant, 22 Vul deviates significantly in the sense that the empirical mass loss rate is much larger than predicted.

We conclude on the basis of this (admittedly rather small) sample that our predicted mass loss rates for A-supergiants agree well with the empirical mass loss rates. The situation is unclear for F & G-supergiants. The empirical mass loss rate of 22 Vul (G3 Ib-II) is significantly higher than predicted. The large episodic mass loss rates of ρ Cas and HR 8752 cannot be explained by the radiation driven wind models. So, *unless* the radiation pressure in the winds of F and G stars is much larger than calculated by Abbott (1982), it seems that the mass loss cannot be explained by radiation driven wind models.

7.2. Comparison between observed and predicted terminal velocities

The predicted terminal velocities are compared with the observed values in Fig. 11. The predicted values of v_∞ are esti-

Table 4. The published observed $\dot{M}$ and v_∞ and the predicted values from our model

HD	Sp. Type	$T_{\rm eff}$ [K]	$R_\star$ [$R_\odot$]	$M_\star$ [$M_\odot$]	$\log(L_\star/L_\odot)$	$v_{\rm esc}$ [km s^{-1}]	observed v_∞ [km s^{-1}]	observed $\log \dot{M}$ [$M_\odot$ yr^{-1}]	predicted v_∞ [km s^{-1}]	predicted $\log \dot{M}$ [$M_\odot$ yr^{-1}]
21389	A0 Iae	9730	104.2	14.0	4.9	226		-6.38[1]	589	-6.20
92207	A0 Iae	9730	143.8	22.0	5.2	242	200 ± 30		628	-5.85
223960	A0 Iae	9730	104.2	14.0	4.9	226	120 ± 20		589	-6.20
46300	A0 Ib	9730	34.5	9.5	4.0	324	180 ± 30		843	-7.84
87737	A0 Ib	9730	39.5	10.0	4.1	311		-7.33[1]	808	-7.64
12953	A1 Iae	9230	146.4	19.0	5.1	222	170 ± 20	-6.10[1]	578	-6.10
14433	A1-3 Ia	9080	107.6	17.0	4.9	245	150 ± 50		638	-6.66
197345	A2 Iae	9080	195.8	24.0	5.4	216	200 ± 30	-6.16[1]	562	-5.83
14489	A2 Ia	9080	141.9	20.0	5.1	232	150 ± 20	-6.28[1]	603	-6.28
207260	A2 Ia	9080	98.2	16.0	4.8	249	150 ± 20		648	-6.78
62623	A2 Iab	9080	81.6	15	4.6	265	150 ± 50		689	-7.05
223385	A3 Iae	8770	212.9	25	5.3	212	180 ± 20		550	-5.98
17378	A5 Ia	8510	173.1	20.0	5.1	210	180 ± 30	-6.49[2]	546	-6.48
59612	A5 Ib	8510	45.5	9.5	4.0	282	180 ± 20	-8.52[3]	734	-8.33
85123	A8 Ib	7950	49.8	9.4	3.9	268	200 ± 30		698	-8.86
22 Vul	G3 Ib-II	5100	40	5.0	3.0	218	160 ± 20	-8.22[4,5]	336	-13.96

Remark :
(1) from Barlow & Cohen (1977)
(2) from Lamers, Stalio & Kondo (1978)
(3) from Praderie, Talavera & Lamers (1980)
(4) from Ake & Parsons (1985)
(5) from Reimers & Che-Bohnenstengel (1986)

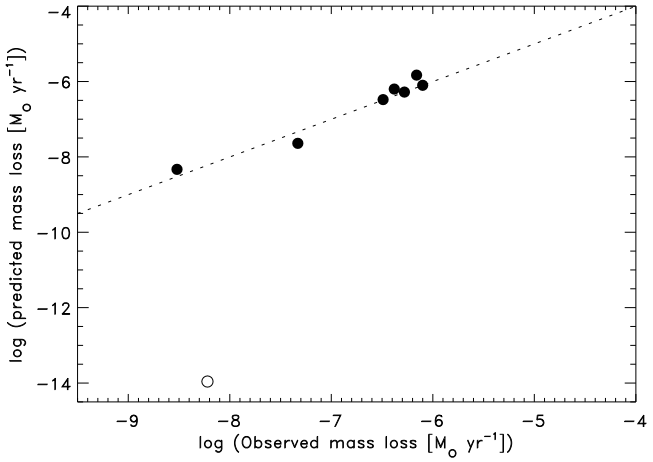

Fig. 10. The observed mass loss rates of A-type supergiants (filled circles) and one G-supergiant (open circle) as compared to the predicted ones. The dotted-line is the one-to-one relation.

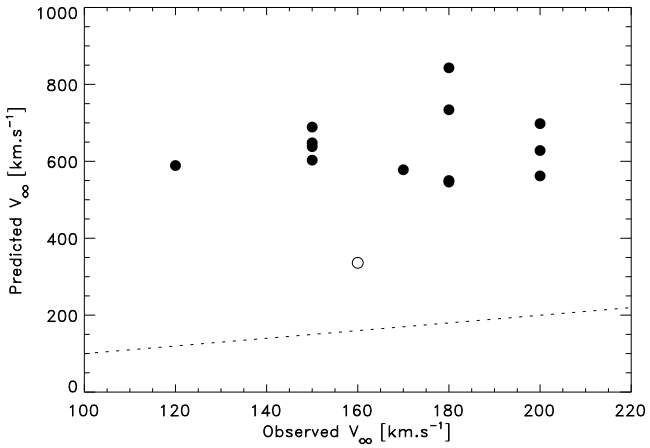

Fig. 11. The comparison between the predicted and observed values of v_∞. The filled circles are for A-supergiants and the open circle is for the G-supergiant. The dotted line is the one-to-one relation. The predicted v_∞ is clearly higher than the observed values by about a factor 3.5.

mated roughly by using :

$$v_\infty = \begin{cases} 2.6 \cdot v_{\rm esc} & \text{for } T_\star > 7500\,{\rm K} \\ (-0.53 + 4.06 \cdot 10^{-4} T_\star) v_{\rm esc} & \text{for } T_\star \leq 7500\,{\rm K} \end{cases} \quad (25)$$

which are the least-square fits from data in Fig. 9.

The predicted terminal velocities, which have accuracy of better than 20 %, are clearly higher than the observed values by about a factor 3.5. In fact, the observed terminal velocities are only about 0.7 times the escape velocities, whereas the pre-

dicted ratios are about 2 to 2.5. We have shown in Sect. 6.2 that the observed terminal velocities may be smaller than the predicted values if $\dot{M}/(R_\star v_\infty) < 10^{-13}$ because the Mg II lines do not reach the terminal velocity. For a stellar radii of about $100\,R_\odot$ and predicted terminal velocities of about $700\,\mathrm{km\,s^{-1}}$, the observed velocity will be smaller than the predicted one if $\dot{M} \leq 7 \cdot 10^{-9}\ M_\odot\ \mathrm{yr}^{-1}$. The mass loss rates of A-supergiants with $\log L_\star > 4.2$ are higher than this value. So the large discrepancy between the observed and predicted terminal velocities are not due to the fact that the Mg II lines do not reach the terminal velocity of the wind.

The alternative explanation for the large discrepancy between the observed and predicted terminal velocities involves a correction of the force multiplier α. Since v_∞ is proportional to $\sqrt{\alpha/(1-\alpha)}$ (Eq. 22), the easiest way to reduce the calculated v_∞ is by artificially reducing the value of α as has been suggested by Lamers et al. (1995). Reducing α means that weak lines are more important in driving the wind than found by Abbott (1982) in his calculation of the force multiplier parameters. Assuming for simplicity a predicted ratio of $v_\infty/v_{\rm esc} \simeq 2\sqrt{(\alpha)/(1-\alpha)}$ and an observed ratio of $v_\infty/v_{\rm esc} \simeq 0.70$ we conclude that α must be about 0.11, which is much smaller than Abbott's values by a factor of 5. But such small values of the force multiplier α makes the predicted mass loss rates is drastically reduced. In order to keep the agreement between the predicted and observed mass loss rates, the value of the force multiplier k has to be increased by a factor of 30 to 40. If this were the case, the excellent agreement between the predicted and observed mass loss rate for A-supergiants would then be fortuitous. This is not a very likely explanation.

8. Summary and conclusion

We have constructed hydrodynamic model atmospheres and radiation driven wind models for A, F and G-supergiants to investigate whether the observed mass loss rates of these stars can be due to radiation pressure. The main assumptions used in modeling the hydrodynamical atmospheres are :

(1) The temperature structure, $T(\tau)$, is taken from line-blanketed and plane-parallel model of Kurucz (1992). We have shown that this $T(\tau)$ is a good approximation to that of a line-blanketed and extended atmosphere calculated Plez (1994).

(2) The ionization in the photosphere and the subsonic part of the atmosphere is assumed to be in LTE.

(3) The radiation pressure due to lines and continua in the subsonic region of the atmosphere is calculated with the assumption that the ratio of the flux-mean opacity ($\overline{\kappa}_{\rm F}$) to the Rosseland-mean opacity ($\kappa_{\rm Ross}$) is a function of optical depth. This function is derived from line blanketed plane-parallel model atmospheres of Kurucz (1992).

(4) The radiative acceleration in the supersonic part of the atmosphere is assumed to be due to lines only. The line radiation pressure is calculated with the force multiplier formalism from Abbott (1982) for a point source star, with the correction for the finite disk from Pauldrach et al. (1986) included.

(5) The density structure is coupled to the velocity structure by the equation of mass continuity.

(6) The Rosseland optical depth of 2/3 is reached at a layer where $T(r) = T_{\rm eff}$.

Using these expressions for the temperature structure and the radiative acceleration, we derived the velocity structure, the density and the mass loss rates of the model atmosphere by solving the momentum equation. From this study we can draw several conclusions :

a. The high opacity and the large radiation pressure of the H-ionization zone in the subsonic region does not give influence on the overall mass loss rate. For the stars with mass loss rates of $\dot{M} \lesssim 6\ 10^{-5}\ M_\odot\ \mathrm{yr}^{-1}$, the high opacity in the H-ionization zone produces a pressure inversion in the atmosphere because the net force is directed outwards in that zone and the momentum equation is approximately equal to the hydrostatic equation in the subsonic region. For higher mass loss rates the pressure inversion disappears.

b. Our hydrodynamical models for line driven winds of stars in the range of $5500 \leq T_{\rm eff} \leq 9500$ K have mass loss rates in the range of 10^{-9} to $10^{-5}\ M_\odot\ \mathrm{yr}^{-1}$. The models predict a strong correlation between the mass loss rate and the stellar parameters, with $\log \dot{M} = f(T) + 1.636 \log L_\star$ (Eq. 15) and $f(T)$ given in Table 3, or with the relation of Eq. (19).

c. The predicted mass loss rates of the A-type supergiants agree very well with the observed rates. This strongly suggests that the winds of these stars are driven by radiation pressure. There are no reliable empirical mass loss rates for F-supergiants to be compared with our prediction.

d. Our hydrodynamical models show that the velocity law of the radiation driven winds of A, F & G-supergiants fits very well to a β-law with $\beta = 0.80$.

e. The terminal velocities are about a factor three too high as compared to the observed values. This can be explained in two ways: either the effective escape velocity of the stars is much smaller than we adopted or the force multiplier parameters for these stars are very different from the adopted values.

(1.) A reduction of the photospheric escape velocity by a certain factor would decrease the predicted values of v_∞ by the same factor, but it would increase the predicted mass loss rate. This is because v_∞ is directly proportional to $v_{\rm esc} \sim {M_{\rm eff}}^{1/2}$ and $\dot{M}$ is proportional to ${M_{\rm eff}}^{(\alpha-1)/(\alpha)} \sim {M_{\rm eff}}^{-1}$ (see Eq. 19). So reducing the effective escape velocity by a factor 3 would imply an reduction of the effective mass by a factor 9 and an increase of the predicted mass loss rate by a factor 9. Such a drastic reduction of the effective mass does not seem likely. Moreover it would spoil the excellent agreement between predicted and observed mass loss rates.

(2.) The explanation of the discrepancy of a factor three between the low observed and the high predicted values of v_∞ in terms of a change in α requires a reduction of α from about 0.5 to a value as small as 0.11 (see Sect. 7.2). However, such a constant low value of α would also result in a drastic decrease the predicted mass loss rates which would destroy the excellent agreement between the observed and predicted mass loss rates. In that case the force multiplier k also has to be adjusted by a large factor

to bring the predicted mass loss rates into agreement with the observations. The excellent agreement between the predicted and observed mass loss rate for A-supergiants would then be fortuitous. This is not a very likely explanation.
(3.) The remaining solution to this problem is the assumption that α is not constant, but decreases outwards from about 0.5 just above the photosphere, to a much smaller value at larger distances. This is because the mass loss rate is set by the radiation pressure in the lower part of the wind just above the photosphere, whereas the terminal velocity is determined by the radiation pressure at larger distances. Such a change in the force multiplier parameter α might be due to two effects: firstly, the low temperature in the wind may result in a significant change in the ionization of the wind with distance which would change the radiation force. Secondly there may be a decoupling of the wind driving ions from the remainder of the gas at the low densities in the winds. If the density in the wind drops below some critical value, the ions that are accelerated by radiation pressure experience insufficient Coulomb interactions with the ambient gas. This results in very high velocities of the line-driven ions (and very low optical depths of their lines) and in a slow acceleration (small α) and low terminal velocities of the rest of the gas. This effect was estimated by Lamers & Morton (1976) and by Springmann & Pauldrach (1993) for O-stars, and by Babel (1995) for A-stars.

f. The observed mass loss rate of the G-supergiant 22 Vul is a factor 10^5 higher than the predicted by radiation driven winds. This is not surprising because G-supergiants have a hybrid structure. The studies of e.g. α and β Aqr have shown that the Ca II line emission and the high excitation lines in the UV indicate the presence of chromospheres, whereas the presence of blue shifted components of e.g. Mg II and Ca II lines indicate substantial mass loss (Hartmann et al. 1980, Dupree & Reimers 1987, Pasquini et al. 1988). Our calculations do not take into account the possible presence of a chromosphere.

g. It would be very interesting to compare our predicted mass loss rates with observed rates for F-supergiants, to see at which spectral type or luminosity the agreement between predictions and observations that we found for A stars changes into the disagreement that we found for the G-supergiant. If the discrepancy starts at the same spectral type where the chromospheric emission becomes noticeable, it would indicate that the break-down of the radiation driven wind models is due to the presence of a chromosphere. Unfortunately, we could not find reliable mass loss rates or terminal wind velocities for normal F-type supergiants in the literature.

h. Our models of the hydrodynamical atmospheres show that the velocity gradient in the region where $\log \tau_{\rm Ross} \simeq -2$, is still very small and the density structure of the hydrodynamic model is very similar to that of the hydrostatic model if the mass loss rate is less than about $10^{-7}\ M_\odot\ {\rm yr}^{-1}$. This implies that the weaker photospheric lines will not be affected by the outflow of the atmosphere. However the very strong lines, formed at $\log \tau_{\rm Ross} < -5$ will be affected by the velocities: they will be violet shifted and broadened by the velocity gradient in the upper atmosphere. For stars with mass loss rates higher than about $10^{-6}\ M_\odot\ {\rm yr}^{-1}$ the weaker lines may be affected by the velocity gradient in the line forming region. This effect can easily be mistaken for evidence of large turbulent velocities (Lamers & Achmad, 1994).

In a forthcoming paper we will use these hydrodynamical models for the analysis of high resolution and high S/N optical spectra of A, F and G-supergiants obtained at ESO, to investigate the effects of the mass loss on the optical spectrum.

Acknowledgements. L.A. gratefully acknowledges financial support from the Indonesian government and the ESO Studentship program. He thanks Thomas Augusteijn for very fruitful discussions. We thank the referee for his constructive comments.

References

Abbott, D. C. 1982, ApJ, 259, 282
Ake, T. B., Parsons, S. B. 1985, ApJ. 298, 772
Babel, J. 1995, A&A 301, 823
Barlow, M. J., Cohen, M. 1977, ApJ 213, 737
Castor, J. I., Abbott, D. C., and Klein, R. I. 1975, ApJ, 195, 157
de Jager, C., Nieuwenhijzen, H. and van der Hucht, K. A. 1988, A&AS 72, 259
Dupree, A. K., Reimers, D. 1987, in Y. Kondo (ed.) *Exploring the Universe with the IUE Satellite*, p. 321
Friend, D., Abbott, D. C. 1986, ApJ 311, 701
Hartman, L., Dupree, A. K., Raymond, J. C. 1980, ApJ 236, L143
Kudritzki, R. P., Pauldrach, A., Puls, J., Abbott, D. C. 1989, A&A 219, 205
Kurucz, R. L. 1992, ATLAS 6 program
Lamers, H. J. G. L. M., Achmad, L. 1994, A&A 291, 856
Lamers, H. J. G. L. M., Morton, D. C. 1976, ApJS. 32, 715
Lamers, H. J. G. L. M., Snow, T. P., Lindholm, D. M. 1995, ApJ 455, 269
Lamers, H. J. G. L. M., Stalio, R. and Kondo, J. 1978, ApJ 223, 207
Maeder, A. 1992, in *Instabilities in Evolved Super- and Hypergiants*, eds. C. de Jager & H. Nieuwenhuijzen, North-Holland, p. 138
Maeder, A., Meynet, G. 1988, A&AS 76, 411
Pasquini, L., Pallavicini, R. and Pakull, M. 1988, A&A 191, 253
Pauldrach, A., Puls, J., Kudritzki, R. P. 1986, A&A 164, 86
Plez, B. 1994, private communication
Praderie, F., Talavera, A. and Lamers, H. J. G. L. M. 1980, A&A 86, 271
Reimers, D. 1989 in "FGK Stars and T Tauri stars", NASA-SP 502, eds. L.E. Cram and L.V. Kuhi
Reimers, D., Che-Bohnenstengel, A. 1986, Astr. Ap. 166, 252
Springmann, U. W. E., Pauldrach, A. W. A. 1993, A&A 262, 515
Wessolowski, U., Schmutz, W., Hamann, W.-R. 1988, A&A 194, 160

This article was processed by the author using Springer-Verlag LaTeX A&A style file *L-AA* version 3.